ACS Sustainable Chemistry & Engineering

pubs.acs.org/journal/ascecg

Research Article

Tailoring the Electrochemical Interface for 5-Hydroxymethylfurfural Hydrodimerization Using Single and Gemini Quaternary Ammonium Surfactants

Mohammad Peirow Asfia, Julien Steffen, Angelina Cuomo, Urban Sajevic, Andreas Görling, Karl J. J. Mayrhofer, and Pavlo Nikolaienko*

Cite This: ACS Sustainable Chem. Eng. 2025, 13, 17151−17160

Read Online

ACCESS | Metrics & More | Article Recommendations | Supporting Information

ABSTRACT: The electrochemical pinacol coupling of 5-hydroxymethylfurfural (HMF) offers a sustainable route to value-added chemicals, yet optimizing selectivity and conversion remains a challenge. Therefore, we employed surfactants as electrode−electrolyte interface modifiers to enhance the electro-hydrodimerization of HMF to 5,5′-bis-(hydroxymethyl)hydrofuroin (BHH) on carbon electrodes. By applying 10 mM long-chain quaternary trimethylammonium surfactants, we successfully enhanced the product selectivity toward BHH from 37% to almost 60%. Replacing single-charged surfactants with analogous Gemini surfactants lowers the required modifier concentration to only 0.2 mM while maintaining the same results. Furthermore, substituting planar glassy carbon electrodes with reticulated vitreous carbon (RVC) enables a significant increase in HMF conversion, exceeding 96% within 2 h, with no performance loss. This study provides new insights into surfactant-mediated electrocatalysis and establishes a scalable strategy for enhancing electrochemical biomass valorization.

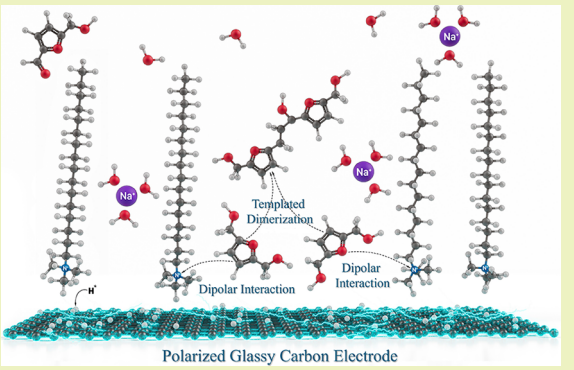

KEYWORDS: *5-Hydroxymethylfurfural, Gemini surfactants, carbon materials, electrode−electrolyte interface, biomass upgrade*

INTRODUCTION

Within the modern agenda to replace fossil-based feedstock for fuels and chemicals, the utilization of biomass has received interest as a sustainable and "defossilized" alternative, with lignocellulose as the cheapest and most abundant material.[1−5] 5-Hydroxymethylfurfural (HMF),[6,7] derived from lignocellulose, ranks among the most important biomass-derived platform chemicals,[8] serving as a key intermediate for producing polymer precursors,[9−11] fine chemicals,[12−14] fuels, and fuel precursors.[7,15−18] One such product, 5,5′-bis-(hydroxymethyl)hydrofuroin (BHH), formed through pinacol C−C coupling of HMF, has a C_{12} structure with promising properties for use as diesel or a jet fuel precursor.[19−25]

In recent years, electrochemical approaches have gained attention to mitigate the intermittent nature of renewable electricity sources and as a technology for decentralized and energy-efficient production processes.[26] In light of this, HMF, a crucial building block for organic electrosynthesis, and its electrochemical reduction products show long-standing development prospects.[27] Using water as a proton source, although advantageous in practical aspects, poses challenges due to the competing hydrogen evolution reaction (HER), lowering HMF conversion and Faradaic efficiency (FE).[28,29] Utilizing cathode materials with high hydrogen overpotential like carbon mitigates the HER, but achieving selectivity toward target products remains challenging.[20] While the development of electrocatalysts with specialized structures leads to improved electrochemical performance,[30−32] modulating the electrocatalytic reaction processes via modification of the electrode−electrolyte interfaces is an emerging strategy.[33,34] For example, metal cations,[20] organic molecules,[35,36] and cationic surfactants[33,34] at the electrode−electrolyte interface can affect species transfer and distribution, thereby impacting reaction activity toward the target product. Quaternary ammonium cationic surfactants stand out as highly effective additives for steering product distribution in various electrochemical applications.[37,38] Kong et al.[34] reported a microenvironment regulation strategy by modifying carbon paper with hexadecyltrimethylammonium bromide (CTAB) cations, which enhanced the electrochemical carbon−carbon coupling of benzaldehyde with improved activity and racemate stereo-

Received: May 8, 2025
Revised: September 25, 2025
Accepted: September 25, 2025
Published: October 10, 2025

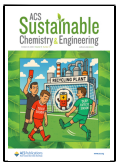

selectivity. Zhang et al.[33] studied the electrocatalytic hydrogenation of HMF to 2,5-bis(hydroxymethyl)furan (BHMF) on a RhCu catalyst, facilitated by the presence of CTAB as an electrode−electrolyte interface modifier.

Previous studies by our group have revealed glassy carbon (GC) as the electrode material of choice for the electrochemical hydrodimerization of HMF to BHH at practical reaction rates. Aside from the effects of applied potential and initial HMF concentration on product distribution,[19] we also investigated the impact of the supporting electrolyte's cation identity on the electrochemical hydrodimerization and hydrogenation of HMF and proposed a reaction mechanism.[20] Despite our comprehensive studies, reinforced by Choi's reports on the effect of electrolyte pH,[39] the current protocol for electrochemical reduction of HMF on glassy carbon toward BHH formation still lacks selectivity and requires out-of-the-box strategies to face such a challenge.

In this study, we utilized quaternary ammonium surfactants with varying alkyl chain lengths as electrolyte additives to improve the electrochemical reduction of HMF and enhance its conversion to BHH on a glassy carbon electrode. Real-time mass spectrometry (RTMS) and long-term preparative electrochemistry measurements, coupled with quantitative analysis, demonstrated that these additives increase the selectivity toward BHH. Additionally, the modifiers shifted the onset potential of HMF reduction to more positive values, enabling optimal selectivity at lower applied potentials. *Gemini* surfactants, prepared upon linking trialkyl amines with terminal dibromo alkanes, achieved similar results as monocharged ones but at significantly lower concentrations. We verified these trends in selectivity with periodic density-functional theory (DFT) calculations of suitable model systems. Furthermore, reticulated vitreous carbon (RVC) foam as the cathode material further increases the conversion rate.

RESULTS AND DISCUSSION

As a setup, we employed an electrochemical real-time mass spectrometry (EC-RTMS) screening setup comprising a V-shaped microfluidic screening flow cell (SFC) with an opened bottom channel for fast relocation to an unexposed working electrode spot for reproducibility and statistics, coupled to a direct mass spectrometer through a sipping capillary and liquid−vapor interphase. This platform, which general scheme is depicted in Figure 1a, allows instantaneous detection of reaction products, enabling experimentations under dynamic operations.[40] In contrast to steady-state testing in batch, with EC-RTMS, subtle reaction transients can be discovered over potential- or time-resolved monitoring of target m/z-ratios, plotted as volt-massograms.

According to the previously optimized conditions,[20] we fixed a solution of 20 mM HMF in 0.1 M sodium carbonate buffer as the blank condition. We used 10 mM quaternary ammonium salts as modifiers under hydrodynamic conditions by applying a flow rate of 0.5 mL min^{-1}. As can be seen in Figure 1b and c, an electrochemical protocol comprising a voltammetry sweep between −0.1 V and −1.0 V vs E_{RHE}, followed by five consecutive potential holds (at −0.6 V, −0.7 V, −0.8 V, −0.9 V, and −1.0 V vs E_{RHE}) was performed within time-resolved product formation monitoring. When only sodium carbonate buffer is present in the electrolyte, upon increasing the negative overpotential, the BHH formation reaches a maximum at −0.8 V vs E_{RHE} and then slightly fades due to competing HER and BHMF formation. However, when

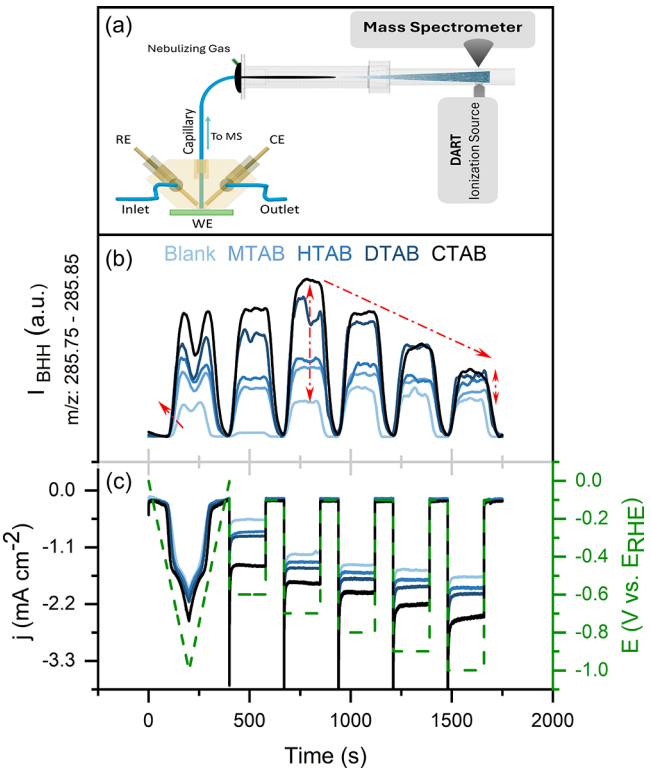

Figure 1. Schematic of the RTMS setup (a), RTMS-derived surfactant-stacked voltmassograms of BHH formation (b), and overall current density and applied potential (c). Electrolyte: 20 mM HMF, 10 mM surfactants in 0.1 M sodium carbonate buffer (pH 9.2), working electrode: glassy carbon.

trimethylammonium surfactants (Supporting Information, Table 1) are present, the BHH formation is profoundly enhanced, with the maximum production at a less negative applied potential of −0.7 V vs E_{RHE}.

However, a further increase of the overpotential does not increase the BHH formation but becomes even more detrimental at potentials more negative than −0.9 V vs E_{RHE}. Even though the current density continues to increase with increasing potential, HER and the 2-electron hydrogenation of HMF to BHMF start to dominate over the 1-electron dimerization process. This potential dependent competition between HER, BHMF, and BHH formation of HMF the reduction reaction (HMF-RR) was already observed and mechanistically studied by Kloth et al.[19,20]

Moreover, the surfactants' enhancing effect on BHH formation is most pronounced at potentials around −0.7 V vs E_{RHE} and also decreases with higher overpotential. It is further dependent on the alkyl chain length of the surfactants. BHH formation enhancement is most effective in the presence of longer alkyl chains like hexadecyltrimethylammonium bromide (CTAB) or decyl trimethylammonium bromide (DTAB). The effect of shorter-chain surfactants such as hexyltrimethylammonium bromide (HTAB) is slightly higher than that of nonsurfactant tetramethylammonium bromide (MTAB).

Further insights into the effect of CTAB on the electrochemical behavior of HMF on glassy carbon were gained under stagnant conditions of cyclic voltammetry (CV) (Figure 2a, and magnified enclosure at Figure 2b, and Figure 2c) at varied scan rates. The expected decrease in peak current upon shifting

https://doi.org/10.1021/acssuschemeng.5c04330
ACS Sustainable Chem. Eng. 2025, 13, 17151−17160

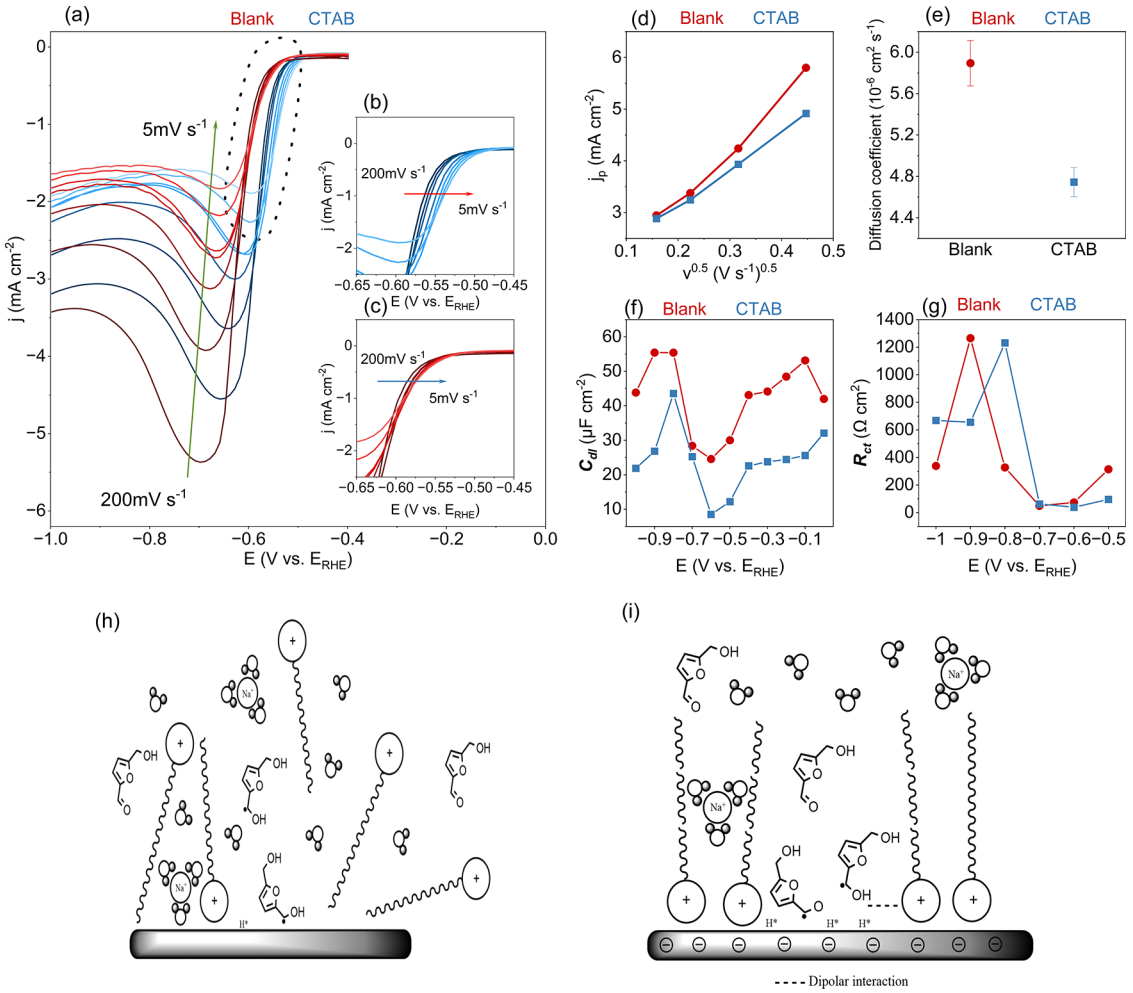

Figure 2. Cyclic voltammograms at different scan rates showing the onset potential of HMF-RR in the absence and presence of 10 mM CTAB (a); onset potential drift at various scan rates with (b) and without (c) presence of 10 mM CTAB; peak current density vs square root of scan rate (d); HMF diffusion coefficient derived from the Randles−Ševčík equation (e); double layer capacitance potential dependency (f); resistance of the charge transfer potential dependency (g); schematic representation of HMF, CTAB, sodium cations, and water molecular configurations near the surface of glassy carbon with no polarization (h), and with applied negative potential (i) (not to scale).

the scan rate from 200 to 5 mV s^{-1} is visible for both CTAB-containing and blank electrolytes. A decrease in the onset potentials with a decreasing scan rate is more prominent in the presence of CTAB, suggesting not only HMF adsorption events but also the formation of a dynamic CTAB layer. The formation of the latter is expected to be time-dependent and more uniform over a slower potential change.

Notably, the peak current−scan rate dependency, derived from the Randles−Ševčík equation for irreversible electrochemical processes (Figure 2d), is more linear for the CTAB-containing electrolyte, while blank electrolyte behavior suggests a change in the number of electrons involved in the electron transfer. Although it is in the same order of magnitude, the diffusion coefficient of HMF in the presence of CTAB is slightly smaller, further contributing to the hypothesis of a dynamic film formation at the inner Helmholtz plane layer (Figure 2d and e).

The properties of the CTAB-tailored electrochemical interface of glassy carbon were probed by electrochemical impedance spectroscopy (EIS). According to the known behavior of surfactants upon electrode polarization,[34] a transition between two distinct tail-to-surface and head-to-surface orientations is expected for CTAB in water. At the same time, the presence of alkali cations as major electrochemical double-charged layer components and the presence of HMF-derived adsorbates make the properties of the electrode microenvironment complex and dynamic.[20] As can be seen in Figure 2f and g, potential-resolved values for both double-layer capacitance (C_{dl}) and charge transfer resistance (R_{ct}) follow a similar trend regardless of the presence of the surfactant. Nevertheless, the C_{dl} for the CTAB-modified interface is globally lower, suggesting a contribution of the aliphatic chain length in charge separation and low dielectric permittivity. The values for R_{ct} show a sharp increase within the applied potential. This effect occurs at a potential more negative than −0.8 V for blank compared to −0.7 V vs E_{RHE} for CTAB, aligning with the experimental SFC data.

Figure 2h and i shows how CTAB and Gemini surfactants arrange at the electrode−electrolyte interface under different conditions. Without an applied potential (Figure 2h), the surfactant molecules orient with their hydrophobic tails toward the carbon surface and their hydrophilic headgroups facing the electrolyte, forming an interfacial layer. When we apply a negative potential (Figure 2i), the surfactant layer reorganizes in response to the electrode charge, which changes the local distribution of the ions and reactants. The observed minimum

https://doi.org/10.1021/acssuschemeng.5c04330
ACS Sustainable Chem. Eng. 2025, 13, 17151−17160

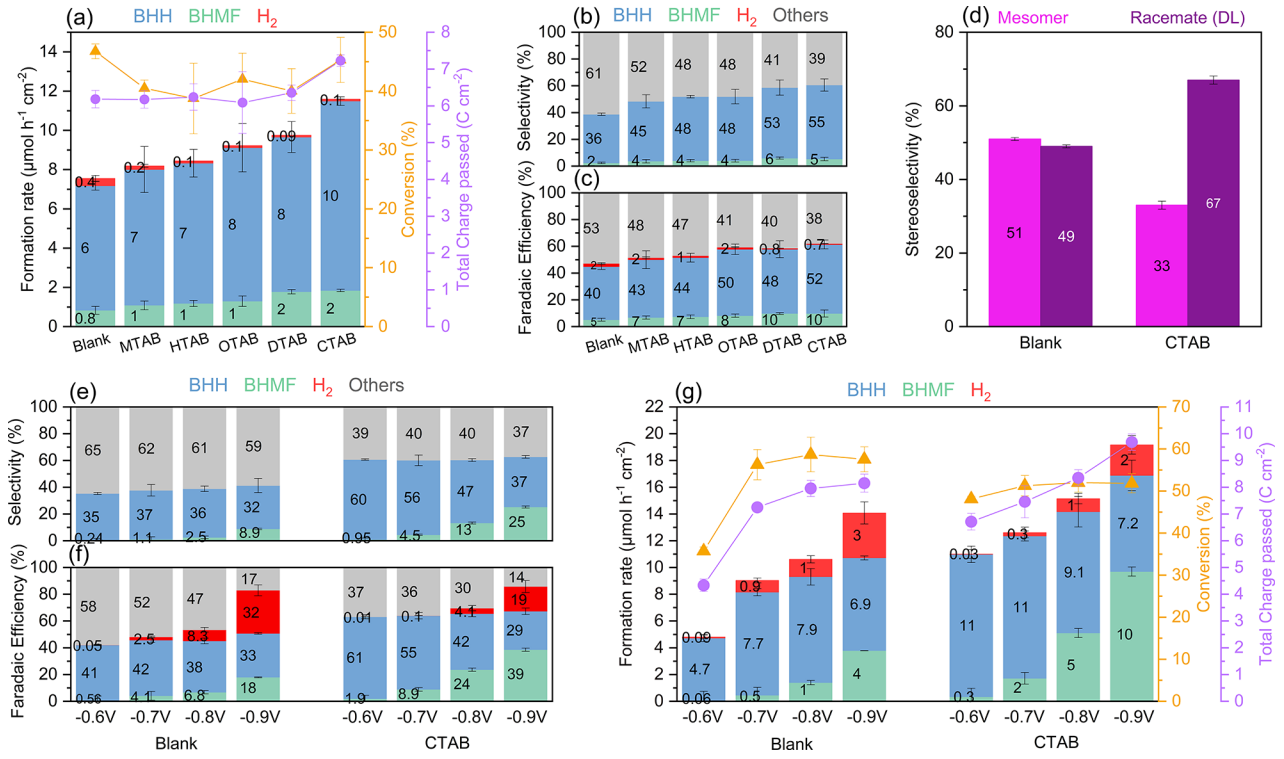

Figure 3. Steady-state electrolysis of 20 mM HMF in the presence of different RMe_3N^+ surfactants (10 mM) during 2 h of electrosynthesis. HMF conversion (triangles), total charge passed (circles), and formation rates (columns) (a); selectivity (b) and Faradaic efficiency (c) of BHH, BHMF, and H_2; stereoselectivity of BHH (d) obtained at −0.7 V vs E_{RHE}. Selectivity (e), Faradaic efficiency (f), average formation rates (columns), HMF conversion (triangles), and total charge passed (circles) (g) of HMF-RR at various potentials on GC. All values are averaged from at least three measurements.

in C_{dl} around −0.6 V vs E_{RHE} to −0.7 V vs E_{RHE} reflects the formation of a structured interfacial layer. In this potential region, $\pi-\pi$ interactions between HMF and the graphitic surface stabilize the ketyl radicals near the electrode, while CTAB molecules organize into a dense and uniform layer. This ordered structure decreases the surface entropy and limits the mobility of solvated ions within the electrochemical double layer. As a result, both the effective ion accessibility and interfacial distance contribute to the reduction in C_{dl}. The compact arrangement also restricts water penetration and proton transfer, further enhancing interfacial selectivity.[41−43]

Our static contact angle measurements (Figure S1) support this interpretation. Adding CTAB or Gemini surfactants (introduced *videinfra*) lowers the contact angle compared to that of the blank electrode, which shows that the modified surface becomes more hydrophilic. This trend confirms that the surfactant headgroups face the electrolyte, consistent with the behavior described by Kong et al.[34] Overall, these results demonstrate that the surfactant layer increases wettability and creates a structured microenvironment that helps control the reactant orientation during HMF electrohydrodimerization.

The observed effects of trimethylammonium surfactants on HMF-RR suggest the possibility of modifying the electrode−electrolyte interface and the electrochemical double-layer features on the surface of glassy carbon. The presence of a hydrophobic tail and a hydrophilic head in these ionic compounds, along with their interaction with the negatively charged electrode and ketyl radical of HMF, helps regulate the microenvironment for pinacol coupling.

Quantitative Validation. To quantify the effect of surfactant modifiers, we conducted long-term chronoamperometry at −0.7 V vs E_{RHE} using an in-house designed preparative divided flow cell (Figure S2),[19,20,42] equipped with in-line HPLC and GC for sample analysis. As such, solutions containing 20 mM HMF and 10 mM RMe_3N^+ surfactants in 0.1 M sodium carbonate buffer were electrolyzed for 2 h under recirculation conditions. As shown in Figure 3a, increasing the quaternary trimethylammonium alkyl chain length enhances the formation rates of both BHH and BHMF. Notably, the HMF conversion remains relatively constant between 40 to 50% over 2 h regardless of the surfactant added, suggesting the HMF-RR to remain mass transport limited. As shown in Figure 3b, the selectivity of BHH increases with the alkyl chain length of the added surfactant. For larger surfactants like CTAB, which repel water molecules from the surface more effectively than the others, BHH selectivity increases from 36% to nearly 55%. These ionic modifiers also reduce the selectivity toward undesired side products ("others"),[20] comprising a complex mixture of humins, formed upon diverse dimerization and polymerization of the HMF and its ketyl radical. A similar trend appears for the Faradaic efficiency of BHH and BHMF as the major products (Figure 3c). Although HER is not the dominant process on glassy carbon, its rate still drops with the presence of surfactants, supporting the suggestion of the depletion of surface populated water molecules. Further investigations were carried out for CTAB due to its superior effect on the BHH selectivity and formation rate enhancement.

Aldehyde-derived pinacols can be formed in four enantiomers, two of which become identical for the same aldehyde dimerization due to a plane of symmetry.[19,20] Therefore, in practice, BHH is detected in two stereoisomeric forms: *meso* and racemate (DL). Figure 3e shows that the DL to *meso* ratio of

https://doi.org/10.1021/acssuschemeng.5c04330
ACS Sustainable Chem. Eng. 2025, 13, 17151−17160

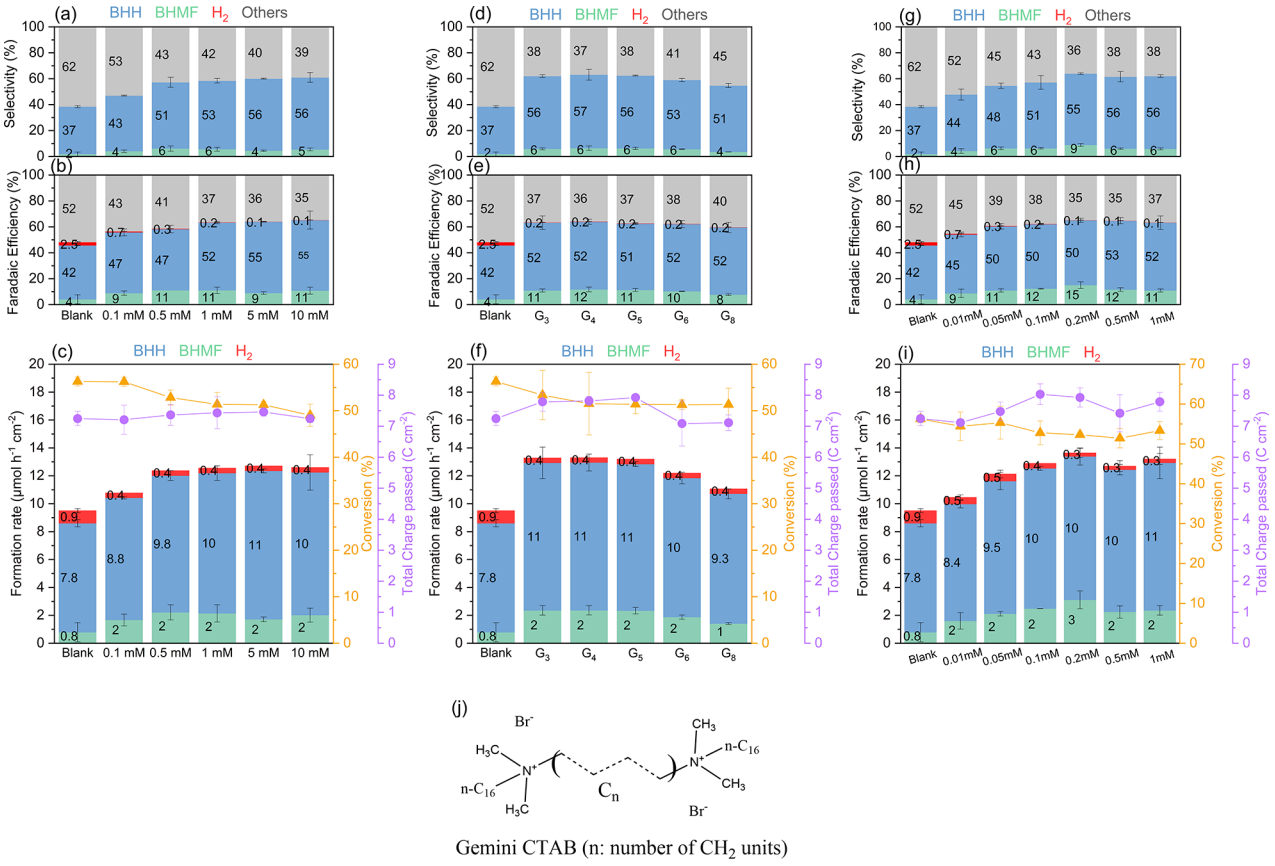

Figure 4. Steady-state electrolysis of HMF on GC, 20 mM HMF in 0.1 M carbonate buffer (pH 9.2), 2 h reaction time at an applied potential of −0.7 V vs E_{RHE}. Selectivity (a), Faradaic efficiency (b), average formation rates (columns), HMF conversion (triangles), and total charge passed (circles) (c) in the presence of different concentrations of CTAB. Selectivity (d), Faradaic efficiency (e), average formation rates (columns), HMF conversion (triangles), and total charge passed (circles) (f) in the presence of *Gemini* CTAB (G_n) with varying chain lengths of the linker (*n*: number of CH_2 units). Selectivity (g), Faradaic efficiency (h), average formation rates (columns), HMF conversion (triangles), and total charge passed (circles) (i) in the presence of various concentrations of *Gemini*-CTAB (G_3), and schematic of the Gemini CTAB (G_n) structure (j). All values are averaged from at least three measurements.

formed BHH is also affected by the presence of CTAB (the corresponding separation of these two stereoisomers in the HPLC chromatogram is shown in the Supporting Information, Figure S3). Notably, the formation rate and selectivity of *meso* BHH remain constant, regardless of the surfactant presence. Therefore, the increased total formation rate and selectivity of BHH are attributed solely to the rise in DL BHH. This observation aligns with the notion of the *meso*-form to be formed upon dimerization of surface flat-adsorbed HMF ketyl radicals through $\pi-\pi$ interactions, while their rate is surface area dependent and remains constant. At the same time, DL racemate is formed upon cation-templated orientation, promoted by the surfactants' ability to stabilize HMF ketyl radicals, ruling out uncontrolled dimerization or polymerization pathways.[34]

To compare the results from EC-RTMS and steady-state measurements, we reinvestigated how the applied potential affects the product distribution. A comparison of plots in the absence and presence of CTAB reveals that the selectivity toward BHH at an applied potential of −0.6 V vs E_{RHE} increases from 35% to 60%, respectively. A similar trend is observed for the Faradaic efficiency, as shown in Figure 3f, emphasizing the positive effects of CTAB on BHH formation. Furthermore, Figure 3g shows that, at −0.6 V vs E_{RHE}, the formation rate of the dimerization product is more than double in the presence of CTAB compared to the blank electrolyte. This is due to the higher conversion rate of HMF and greater total charge passed under these conditions.

However, as shown in Figure 3e, applying more negative potential reduces the effectiveness of these modifiers in enhancing the BHH selectivity. For instance, at −0.6 V vs E_{RHE}, the BHH selectivity in the presence of CTAB is approximately 60%, while at −0.9 V vs E_{RHE}, the selectivity drops to 37%. The observed trend in potential resolved BHH selectivity correlates with the observation in the EC-RTMS results.

Notably, the presence of CTAB also increases BHMF selectivity at −0.9 V vs E_{RHE} from 9% (blank electrolyte) to 25%. This improvement also results from the surfactant stabilizing HMF ketyl radicals near the surface, preventing polymerization. At higher negative potentials, the increased availability of protons near the surface, caused by enhanced Volmer step activity, increases the likelihood of these stabilized ketyl radicals interacting with protons, resulting in increased BHMF formation.

***Gemini* Surfactants.** After investigating the effects of alkyl chain length for monocharged surfactants and applied potential, we examined the effect of CTAB concentration, as shown in Figure 4(a−c). The boosting effect on BHH selectivity with increasing CTAB concentration stops at

https://doi.org/10.1021/acssuschemeng.5c04330
ACS Sustainable Chem. Eng. 2025, 13, 17151−17160

about 5 mM. To overcome this limitation, we sought to increase the number of charged species at the electrode surface without raising the surfactant concentration upon utilizing their *Gemini*-version (Supporting Information, Table 2, Figures S4–S8).[44,45] As such, two CTAB molecules are tethered to a double-charged surfactant by a carbon chain linker between the head groups upon replacement of one of the methyl groups.

Next, we investigated how the linker chain length of *Gemini*-CTABs influences product distribution during HMF-RR. As depicted in Figure 4(d–f), applying *Gemini*- instead of a single CTAB does not significantly impact selectivity, Faradaic efficiency, or the formation rate of products up to medium-sized linkers. However, when the linker length increases to C_6, the BHH selectivity slightly decreases to 51%, favoring the formation of humins ("*others*"). The observed decline in the formation rate might originate from the increased distance between the ketyl radical species stabilized by the positively charged surfactant heads. This greater distance reduces the chances of their interaction, leading to a lower likelihood of forming the dimerization product, BHH. The effect of *Gemini*-CTAB concentration on product distribution (Figure 4g–i) follows the same trend as single CTAB but is far superior in the matter of loading. As such, a concentration down to 0.2 mM *Gemini*-version has nearly the same effect in boosting BHH selectivity during HMF-RR as 10 mM CTAB, showing much higher practicability for higher-scale applications. Future studies could further explore the interfacial dynamics and surface organization of Gemini surfactants, including time-resolved spectroscopic or surface-sensitive techniques, to better understand their superior efficiency at low concentrations.

Computational Simulations. We conducted a series of computational simulations with periodic density-functional theory (DFT) to better understand the mechanism and molecular-level interactions, focusing on how these modifiers affect the interaction between HMF, its ketyl radicals, and the electrode surface.

The optimized structures of the gas phase molecules and cations (Supporting Information Figure 8) and detailed calculation settings are shown in the Supporting Information. Their total energies are listed in SI Table 3. It should be noted that the initial geometry of the BHH molecule was built in two different configurations, one with the central OH groups in the *meso* position and one in the antiposition (DL). The antiposition has a (slightly) lower total energy.

The cations were initiated with linear C_{16} chains, while DFT relaxation kept them in this configuration. With finite temperature, the chains are more flexible and will populate numerous local configurations, which cannot be represented with reasonable computational effort by periodic DFT calculations. However, since the main influence on the electronic structure of the adsorbates is exerted by the positively charged heads, we can safely assume that the general stability trends are not influenced significantly by the assumption of straight chains.

The optimized surface adsorption patterns of the different species are shown in Figure 5. In the first row, the adsorption patterns on a blank graphene model surface are shown. All four species essentially lie flat on the surface with OH groups of the molecules pointing roughly parallel to it. Clearly, all molecules are just physisorbed on the surface. If CTAB cations are added to the unit cells, as shown in the second row, then the adsorption geometries of the molecules change significantly.

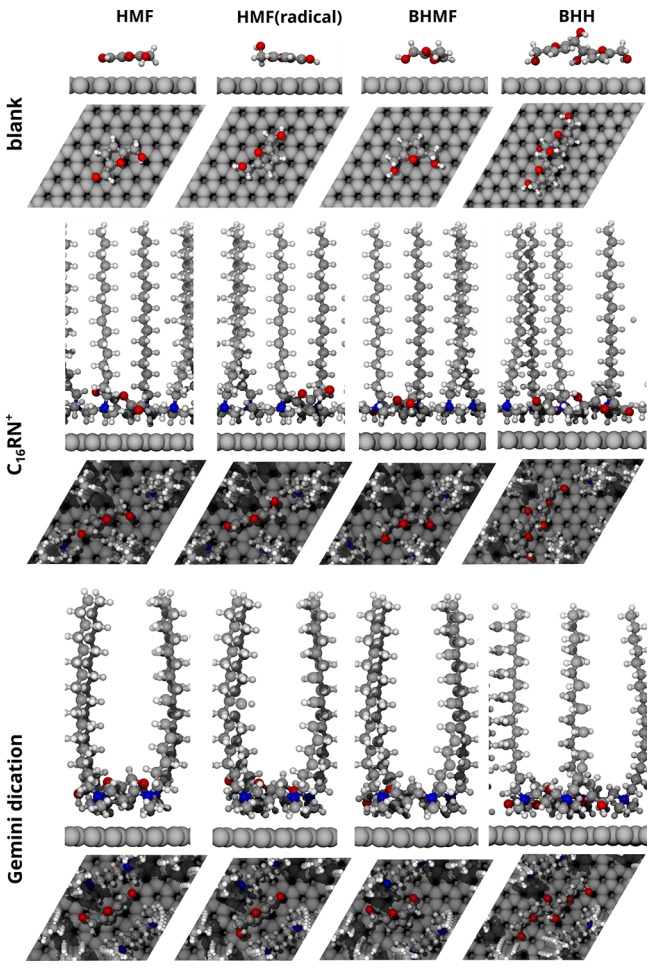

Figure 5. Optimized geometries of HMF and BHH molecules on the graphite model surfaces, with and without coadsorption of C_{16} cations. Each system is shown in two view-directions: top and side. C atoms are gray, H atoms are white, O atoms are red, and N atoms are blue. The graphite C atoms are made larger and diffused to enable an easier distinction of them.

HMF and the ketyl radical of HMF are rotated by almost 90° and point upward with the furfural oxygen atom, whereas the BHMF molecule is partly rotated upward. For the dimer, the furfural oxygen atoms point toward the model surface, still resulting in a raised molecule. Further, most OH groups now point to the graphene surface, probably due to its negative charge, resulting in additional polarization of the group. In the case of *Gemini* C_3 dications (third row), the structures look similar to those with the CTAB cations around them.

Further considering the adsorption energies in Table 1, it can be seen that the HMF molecule and its radical are bound ca. 3.5 times stronger to the surface if CTAB cations are coadsorbed (2.62 and 2.85 eV in comparison to 0.83 and 0.88 eV). The BHMF, on the other hand, is also bound stronger than on the blank model surface but with an energy increase of less than a factor of 2 (1.84 eV instead of 1.02 eV). Thus, coadsorbed CTAB cations result in a significant stabilization of HMF and the HMF radical, being an intermediate in the dimerization. The addition of surfactant cations thus favors the desired dimerization to BHH, which agrees with the higher efficiency observed in the catalytic measurements. The *Gemini* C_3 dications show a similar trend but are even more advantageous for the desired process: The radical is stabilized

https://doi.org/10.1021/acssuschemeng.5c04330
ACS Sustainable Chem. Eng. 2025, 13, 17151–17160

Table 1. Total Energies of the Adsorbed Molecules on the Graphite and Modified Graphite Model Surfaces As Well As Their Adsorption Energies Calculated by Subtracting the Energy of the Combined System from That of the Isolated Parts[a]

system	total energy (eV)	adsorption energy (eV)
HMF, blank	−2114.123055	−0.877866
HMF (radical), blank	−2117.137917	−0.832057
BHMF, blank	−2121.588966	−1.023794
BHH, blank	−2947.121120	−0.902151
HMF, CTAB	−3464.025910	−2.850511
HMF (radical), CTAB	−3466.858209	−2.622139
BHMF, CTAB	−3470.337187	−1.841805
BHH, CTAB	−4295.625744	−2.217087
HMF, *Gemini* G_3	−3481.507134	−2.818306
HMF (radical), *Gemini* G_3	−3484.448852	−2.699353
BHMF, *Gemini* G_3	−3487.648093	−1.639282
BHH, *Gemini* G_3	−4312.908279	−2.481487

[a]By convention, negative adsorption energies indicate thermodynamically stable (favorable) adsorption.

further (2.69 instead of 2.62 eV), and the HMF is slightly destabilized (2.81 instead of 2.85 eV). The increased efficiency of *Gemini* C_3 can thus also be explained by the static DFT calculations. Finally, a similar trend can be seen for the BHH molecule. Its adsorption energy on the blank surface (0.90 eV) is raised to 2.22 eV in the case of coadsorbed CTAB cations and further raised to 2.48 eV in the case of coadsorbed *Gemini* cations. The adsorption energies of *meso* and anticonformations were almost identical, supporting the finding that the racemate BHH is produced preferentially.

The stabilization of adsorbates in the presence of cations is likely due to enhanced bonding of the OH groups to the graphite model surface and to a general polarization of the molecules, also visible by their elevated positions orthogonal to the surface, stabilizing the radical.

The static DFT calculations provide a simplified picture of the overall system, proposing a certain aggregation/density of the cations and neglecting the electrolyte above the cation tails and the complex structure of the glassy carbon.

The significant trends in adsorption energies, however, resulting in changes of more than 1 eV when surfactant cations are added and clearly stabilizing HMF and its radical in comparison to BHMF, are too large to be totally reversed by the mentioned neglected degrees of freedom and thus provide a valuable source of an atomic-resolved understanding of the adsorption processes.

Note that no electric field has been applied in the calculations since even tremendous field strengths of 0.1 V $Å^{-1}$ (corresponding to 1×10^8 V m^{-1}) applied in a preliminary benchmark calculation had almost no impact on the adsorption energies. The cations and induced mirror charges on the upper graphene layer seem to cover the electrostatic effects quite well in the direct vicinity of the surface.

Reticulated Vitreous Carbon As Cathode. While both mono- and double-charged surfactants enhance BHH selectivity as the primary product of HMF-RR on carbon materials, the overall conversion rate remains limited. As shown in Figure 3a, after 2 h of electrolysis at −0.7 V vs E_{RHE}, less than 50% of the initial HMF concentration was converted into products. To address this limitation, we explored using reticulated vitreous carbon (RVC) as the cathode instead of planar glassy carbon (GC), as RVC provides a significantly higher active surface area without requiring a larger electrode setup (Figure S10 in the Supporting Information compares how GC and RVC cathodes affect the product distribution and

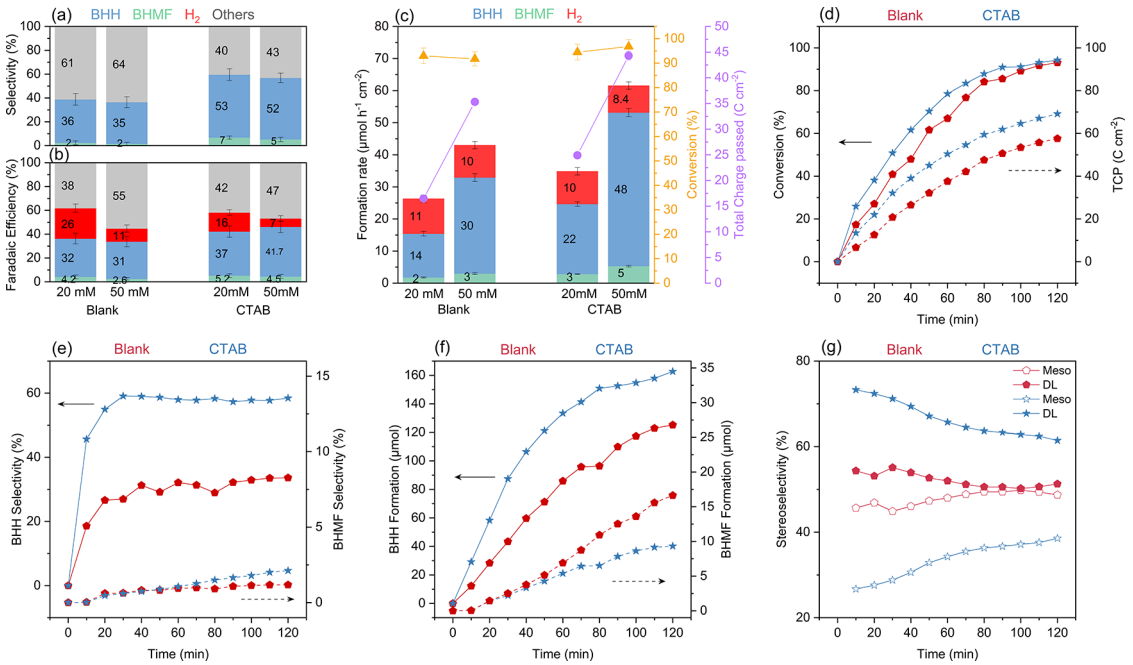

Figure 6. Steady-state electrolysis of HMF on RVC in 0.1 M carbonate buffer (pH 9.2), 2 h reaction time at an applied potential of −0.7 V vs E_{RHE} in the absence (pentagon) and presence of 5 mM CTAB (star). Selectivity (a), Faradaic efficiency (b), average formation (columns), HMF conversion (triangles), and total charge passed (circles) (c) in the absence and presence of 5 mM CTAB, 20 and 50 mM HMF. Conversion (solid) and total charged passed (dash) (d), BHH (solid) and BHMF (dash) selectivity (e), BHH (solid), and BHMF (dash) formation rate (f), and stereoselectivity of BHH (g).

https://doi.org/10.1021/acssuschemeng.5c04330
ACS Sustainable Chem. Eng. 2025, 13, 17151−17160

conversion rate of HMF-RR with 20 mM HMF, with and without 10 mM CTAB). With the implementation of RVC, Figure 6(a–c) shows that while the product distribution remained nearly unchanged, the HMF conversion rate increased to over 96%. Although there was a slight increase in the HER rate, the formation rate of primary products remained favorable compared with planar electrodes. Furthermore, the influence of surfactants on selectivity remained stable, with 5 mM CTAB achieving approximately 53% BHH selectivity alongside full conversion of the initial HMF within 2 h.

With the selectivity and conversion rate under control, increasing the initial HMF concentration from 20 to 50 mM emerged as a potential strategy. Figure 6(a–c) shows that we achieved full conversion within 2 h under these conditions while maintaining consistent BHH selectivity throughout the reaction duration. To further understand how HMF concentration changes over time and its effect on product distribution, semi-online measurements were conducted, with electrolyte samples taken every 10 min.

Figure 6d shows that the reaction converted approximately 80% of the initial HMF concentration within the first 60 min. Over time, as the initial HMF concentration decreased, the overall conversion rate also declined. Figure 6e indicates that BHH selectivity remained nearly constant throughout the experiment, whereas the BHMF selectivity increased progressively. This trend results from the decreasing HMF availability over time; as the HMF concentration lowers, the formation of BHMF increases.[19]

As shown in Figure 6f, the BHH formation rate closely follows that of HMF conversion. During the first hour, the average BHH formation was around 130 μmol. As the reaction progressed and HMF concentration declined, the BHH formation rate also decreased. However, the BHMF formation rate exhibited a steady increase over time.

Finally, as depicted in Figure 6g, the BHH stereoselectivity at the start of the reaction was approximately 90% DL and 10% *meso* in the presence of CTAB. Throughout the electrochemical reaction, this ratio shifted to 60/40%. This trend arises from the initially high HMF concentration, which enhances interactions between surfactant head groups and ketyl radicals, thereby increasing the likelihood of DL formation. As HMF and the corresponding ketyl radical concentrations decrease over time, this interaction becomes less pronounced, leading to a shift in stereoselectivity. Based on the effect of surfactants on HMF-RR over the RVC electrode, maintaining a constant HMF feedstock and optimizing reaction conditions can potentially sustain a consistent 60% BHH selectivity over time, with 80% DL stereoselectivity and a high HMF conversion rate of approximately 80% per hour.

CONCLUSIONS

In summary, we have demonstrated a surfactant-mediated strategy to enhance the electro-hydrodimerization of 5-hydroxymethylfurfural (HMF) to 5,5′-bis(hydroxymethyl)-hydrofuroin (BHH) by precisely tuning the electrode–electrolyte interface. Our findings reveal that *Gemini* surfactants significantly improve efficiency compared to their monocharged counterparts, reducing the needed additive concentration while maintaining high selectivity. Additionally, employing reticulated vitreous carbon (RVC) electrodes dramatically increases HMF conversion, achieving over 96% in just two hours. Notably, the presence of *Gemini* surfactants induces a shift in the stereoselectivity of BHH by modulating the stabilization of radical intermediates and restricting interfacial water access. These surfactants' dual-charged head groups and hydrophobic tails create a structured interface that enhances dipolar interactions, suppresses hydrogen bonding with water, and facilitates a preferential radical coupling pathway. DFT model calculations support these findings and are in agreement with the observed trends. This study underscores the importance of surfactant-driven microenvironment engineering in electrocatalysis and opens new avenues for designing advanced electrode–electrolyte interfaces in biomass valorization and beyond.

EXPERIMENTAL SECTION

Materials and Electrode Preparation. All chemicals, including HMF and quaternary ammonium surfactants, were used as received. Electrolytes were prepared in a carbonate buffer (0.1 M, pH 9.2). Glassy carbon (GC) and reticulated vitreous carbon (RVC) electrodes were used as the working electrodes. Prior to use, GC electrodes were polished with diamond paste and rinsed with ultrapure water.

Electrochemical Measurements. Real-time mass spectrometry (RTMS) was performed in a screening flow cell (SFC) equipped with Ag/AgCl and Pt counter electrodes coupled to a DART–TOF-MS system. Steady-state electrolysis was conducted in a two-compartment flow reactor by using an Ir-MMO counter electrode and a bipolar membrane separator. Cyclic voltammetry (CV) and electrochemical impedance spectroscopy (EIS) were performed under a N_2 atmosphere. Current densities were normalized to the geometric surface area, and all potentials were converted to the reversible hydrogen electrode (RHE) scale.

Product Analysis and Quantification. Liquid-phase products were analyzed via HPLC with UV detection. Gaseous H_2 was quantified by using gas chromatography (GC). HMF conversion, product selectivity, and Faradaic efficiency were calculated based on standard electrochemical equations, as detailed in the Supporting Information.

Surfactant Synthesis. Gemini surfactants were synthesized by refluxing *N*,*N*-dimethylhexadecylamine with dibromoalkanes in acetonitrile for 72 h, followed by purification via recrystallization. Structural confirmation was achieved via a NMR spectroscopy.

Computational Methods. DFT simulations were conducted using VASP with the PBE functional and the D3 dispersion correction. The graphite surface was modeled by using periodic graphene slabs. Adsorption energies were calculated for HMF-derived species in the presence and absence of surfactants. Further computational details are provided in the Supporting Information.

Detailed electrochemical measurement procedures, evaluation methods, and additional data are provided in the Supporting Information.

ASSOCIATED CONTENT

Supporting Information

The Supporting Information is available free of charge at https://pubs.acs.org/doi/10.1021/acssuschemeng.5c04330.

Includes details of materials and chemicals, electrode preparation, electrochemical measurement procedures, and evaluation methods. Provides additional figures, tables, and comparisons supporting the main results, as well as the DFT calculation setup and supplementary data (PDF)

https://doi.org/10.1021/acssuschemeng.5c04330
ACS Sustainable Chem. Eng. 2025, 13, 17151–17160

AUTHOR INFORMATION

Corresponding Author

Pavlo Nikolaienko − *Helmholtz Institute Erlangen-Nürnberg for Renewable Energy (IET-2), Forschungszentrum Jülich GmbH, 91058 Erlangen, Germany;* orcid.org/0000-0002-1508-7589; Email: p.nikolaienko@fz-juelich.de

Authors

Mohammad Peirow Asfia − *Helmholtz Institute Erlangen-Nürnberg for Renewable Energy (IET-2), Forschungszentrum Jülich GmbH, 91058 Erlangen, Germany; Department of Chemical and Biological Engineering, Friedrich-Alexander University Erlangen-Nürnberg, 91058 Erlangen, Germany;* orcid.org/0000-0002-6653-5919

Julien Steffen − *Lehrstuhl für Theoretische Chemie, Friedrich-Alexander-Universität Erlangen-Nürnberg, 91058 Erlangen, Germany;* orcid.org/0000-0001-7933-9557

Angelina Cuomo − *Helmholtz Institute Erlangen-Nürnberg for Renewable Energy (IET-2), Forschungszentrum Jülich GmbH, 91058 Erlangen, Germany; Department of Chemical and Biological Engineering, Friedrich-Alexander University Erlangen-Nürnberg, 91058 Erlangen, Germany*

Urban Sajevic − *Helmholtz Institute Erlangen-Nürnberg for Renewable Energy (IET-2), Forschungszentrum Jülich GmbH, 91058 Erlangen, Germany;* orcid.org/0009-0009-8038-043X

Andreas Görling − *Lehrstuhl für Theoretische Chemie, Friedrich-Alexander-Universität Erlangen-Nürnberg, 91058 Erlangen, Germany; Erlangen National High Performance Computing Center (NHR@FAU), D-91058 Erlangen, Germany;* orcid.org/0000-0002-1831-3318

Karl J. J. Mayrhofer − *Helmholtz Institute Erlangen-Nürnberg for Renewable Energy (IET-2), Forschungszentrum Jülich GmbH, 91058 Erlangen, Germany; Department of Chemical and Biological Engineering, Friedrich-Alexander University Erlangen-Nürnberg, 91058 Erlangen, Germany;* orcid.org/0000-0002-4248-0431

Complete contact information is available at: https://pubs.acs.org/10.1021/acssuschemeng.5c04330

Author Contributions

Mohammad Peirow Asfia, Pavlo Nikolaienko, and Karl J. J. Mayrhofer contributed to the manuscript's writing and the topic's conceptualization. Mohammad Peirow Asfia performed the electrochemical measurements and the analytical quantification. Julien Steffen and Andreas Görling performed the computational simulations and interpretation of the results. Urban Sajevic and Angelina Cuomo contributed to the conceptualization of the topic.

Notes

The authors declare no competing financial interest.

ACKNOWLEDGMENTS

This research has been funded by the Deutsche Forschungsgemeinschaft (DFG, German Research Foundation) under Germany's Excellence Strategy − Exzellenzcluster2186 "The Fuel Science Center" − ID: 390919832. Open Access funding enabled and organized by Projekt DEAL. The authors gratefully acknowledge the scientific support and HPC resources provided by the Erlangen National High Performance Computing Center (NHR@FAU) of the Friedrich-Alexander-Universitat Erlangen-Nürnberg (FAU) under the NHR project b146dc. NHR funding is provided by federal and Bavarian state authorities. NHR@FAU hardware is partially funded by the German Research Foundation (DFG) − 440719683.

REFERENCES

(1) Deng, C.-Q.; Deng, J. Advances of the past 12 years in decarboxylation of biomass carboxylic acids to biofuels and high-value chemicals via photo-or electrocatalysis. *Green Chem.* **2024**, *27*, 275.

(2) Shylesh, S.; Gokhale, A. A.; Ho, C. R.; Bell, A. T. Novel strategies for the production of fuels, lubricants, and chemicals from biomass. *Accounts of chemical research* **2017**, *50* (10), 2589−2597.

(3) Luterbacher, J.; Alonso, D. M.; Dumesic, J. Targeted chemical upgrading of lignocellulosic biomass to platform molecules. *Green Chem.* **2014**, *16* (12), 4816−4838.

(4) Kucherov, F. A.; Romashov, L. V.; Galkin, K. I.; Ananikov, V. P. Chemical transformations of biomass-derived C6-furanic platform chemicals for sustainable energy research, materials science, and synthetic building blocks. *ACS sustainable chemistry & engineering* **2018**, *6* (7), 8064−8092.

(5) Yang, X.; Zhang, Y.; Sun, P.; Peng, C. A review on renewable energy: Conversion and utilization of biomass. *Smart Mol.* **2024**, *2* (4), No. e20240019.

(6) Rosatella, A. A.; Simeonov, S. P.; Frade, R. F.; Afonso, C. A. 5-Hydroxymethylfurfural (HMF) as a building block platform: Biological properties, synthesis and synthetic applications. *Green Chem.* **2011**, *13* (4), 754−793.

(7) Simoska, O.; Rhodes, Z.; Weliwatte, S.; Cabrera-Pardo, J. R.; Gaffney, E. M.; Lim, K.; Minteer, S. D. Advances in Electrochemical Modification Strategies of 5-Hydroxymethylfurfural. *ChemSusChem* **2021**, *14* (7), 1674−1686.

(8) Guo, L.; Zhang, X.; Gan, L.; Pan, L.; Shi, C.; Huang, Z. F.; Zhang, X.; Zou, J. J. Advances in Selective Electrochemical Oxidation of 5-Hydroxymethylfurfural to Produce High-Value Chemicals. *Advanced Science* **2023**, *10* (4), 2205540.

(9) Yang, Y.; Mu, T. Electrochemical oxidation of biomass derived 5-hydroxymethylfurfural (HMF): pathway, mechanism, catalysts and coupling reactions. *Green Chem.* **2021**, *23* (12), 4228−4254.

(10) Chadderdon, X. H.; Chadderdon, D. J.; Pfennig, T.; Shanks, B. H.; Li, W. Z. Paired electrocatalytic hydrogenation and oxidation of 5-(hydroxymethyl)furfural for efficient production of biomass-derived monomers. *Green Chem.* **2019**, *21* (22), 6210−6219.

(11) Zhao, D.; Rodriguez-Padron, D.; Triantafyllidis, K. S.; Wang, Y.; Luque, R.; Len, C. Microwave-assisted oxidation of hydroxymethyl furfural to added-value compounds over a ruthenium-based catalyst. *ACS Sustainable Chem. Eng.* **2020**, *8* (8), 3091−3102.

(12) Gao, Y.; Ge, L.; Xu, H.; Davey, K.; Zheng, Y.; Qiao, S.-Z. Electrocatalytic Refinery of Biomass-Based 5-Hydroxymethylfurfural to Fine Chemicals. *ACS Catal.* **2023**, *13* (17), 11204−11231.

(13) Theerthagiri, J.; Karuppasamy, K.; Park, J.; Rahamathulla, N.; Kumari, M. L. A.; Souza, M. K. R.; Cardoso, E. S. F.; Murthy, A. P.; Maia, G.; Kim, H.-S.; Choi, M. Y. Electrochemical conversion of biomass-derived aldehydes into fine chemicals and hydrogen: A review. *Environmental Chemistry Letters* **2023**, *21* (3), 1555−1583.

(14) Sanghez de Luna, G.; Ho, P. H.; Sacco, A.; Hernández, S.; Velasco-Vélez, J.-J. s.; Ospitali, F.; Paglianti, A.; Albonetti, S.; Fornasari, G.; Benito, P. AgCu bimetallic electrocatalysts for the reduction of biomass-derived compounds. *ACS Appl. Mater. Interfaces* **2021**, *13* (20), 23675−23688.

(15) Bender, M. T.; Yuan, X.; Goetz, M. K.; Choi, K.-S. Electrochemical hydrogenation, hydrogenolysis, and dehydrogenation for reductive and oxidative biomass upgrading using 5-hydroxymethylfurfural as a model system. *ACS Catal.* **2022**, *12* (19), 12349−12368.

(16) Nilges, P.; Schröder, U. Electrochemistry for biofuel generation: production of furans by electrocatalytic hydrogenation of furfurals. *Energy Environ. Sci.* **2013**, *6* (10), 2925−2931.

(17) Jiang, Z.; Zeng, Y.; Hu, D.; Guo, R.; Yan, K.; Luque, R. Chemical transformations of 5-hydroxymethylfurfural into highly added value products: present and future. *Green Chem.* **2023**, *25* (3), 871−892.
(18) Gawade, A. B.; Tiwari, M. S.; Yadav, G. D. Biobased green process: selective hydrogenation of 5-hydroxymethylfurfural to 2, 5-dimethyl furan under mild conditions using Pd-Cs2. 5H0. 5PW12O40/K-10 clay. *ACS Sustainable Chem. Eng.* **2016**, *4* (8), 4113−4123.
(19) Kloth, R.; Vasilyev, D. V.; Mayrhofer, K. J. J.; Katsounaros, I. Electroreductive 5-Hydroxymethylfurfural Dimerization on Carbon Electrodes. *ChemSusChem* **2021**, *14* (23), 5245−5253.
(20) Asfia, M. P.; Cuomo, A.; Kloth, R.; Mayrhofer, K. J.; Nikolaienko, P. The Role of Alkali Cations on the Selectivity of 5-Hydroxymethylfurfural Electroreduction on Glassy Carbon. *ChemSusChem* **2024**, *17*, No. e202400535.
(21) Demirbas, A. The importance of bioethanol and biodiesel from biomass. *Energy Sources, Part B* **2008**, *3* (2), 177−185.
(22) Shang, X.; Yang, Y.; Sun, Y. Electrohydrodimerization of biomass-derived furfural generates a jet fuel precursor. *Green Chem.* **2020**, *22* (16), 5395−5401.
(23) Li, G.; Hou, B.; Wang, A.; Xin, X.; Cong, Y.; Wang, X.; Li, N.; Zhang, T. Making JP-10 superfuel affordable with a lignocellulosic platform compound. *Angew. Chem., Int. Ed.* **2019**, *58* (35), 12154−12158.
(24) Anibal, J.; Xu, B. Electroreductive C-C coupling of furfural and benzaldehyde on Cu and Pb surfaces. *ACS Catal.* **2020**, *10* (19), 11643−11653.
(25) Liu, D.; Chen, E. Y.-X. Integrated catalytic process for biomass conversion and upgrading to C12 furoin and alkane fuel. *ACS Catal.* **2014**, *4* (5), 1302−1310.
(26) Seidler, J.; Strugatchi, J.; Gärtner, T.; Waldvogel, S. R. Does electrifying organic synthesis pay off? The energy efficiency of electro-organic conversions. *MRS Energy Sustainability* **2020**, *7*, No. E42.
(27) Wen, W.; Qiang, L.; Yan, Q.; Zhao, P.; Ma, J.; Liu, C.; He, S.; Zhao, M.; He, Y.; Xiao, H.; Jia, J. Recent advances in electrochemical synthesis of high-value derivatives from 5-hydroxymethylfurfural. *Molecular Catalysis* **2024**, *564*, 114354.
(28) de Luna, G. S.; Sacco, A.; Hernandez, S.; Ospitali, F.; Albonetti, S.; Fornasari, G.; Benito, P. Insights into the Electrochemical Reduction of 5-Hydroxymethylfurfural at High Current Densities. *ChemSusChem* **2022**, *15* (13), No. e202102504.
(29) Lee, D. K.; Kubota, S. R.; Janes, A. N.; Bender, M. T.; Woo, J.; Schmidt, J.; Choi, K. S. The impact of 5-hydroxymethylfurfural (HMF)-metal interactions on the electrochemical reduction pathways of HMF on various metal electrodes. *ChemSusChem* **2021**, *14* (20), 4563−4572.
(30) Wu, Y.; Jiang, Y.; Chen, W.; Yue, X.; Dong, C.-L.; Qiu, M.; Nga, T. T. T.; Yang, M.; Xia, Z.; Xie, C.; Xu, L.; Wang, R.; Wang, S.; Zou, Y. Selective Electroreduction of 5-Hydroxymethylfurfural to Dimethylfuran in Neutral Electrolytes via Hydrogen Spillover and Adsorption Configuration Adjustment. *Adv. Mater.* **2024**, *36* (7), 2307799.
(31) Tian, C.; Yu, J.; Zhou, D.; Ze, H.; Liu, H.; Chen, Y.; Xia, R.; Ou, P.; Ni, W.; Xie, K.; Sargent, E. H. Reduction of 5-Hydroxymethylfurfural to 2, 5-Bis (hydroxymethyl) Furan at High Current Density using a Ga-Doped AgCu: Cationomer Hybrid Electrocatalyst. *Adv. Mater.* **2024**, *36*, 2312778.
(32) Jin, B.; Gao, J.; Zhang, Y.; Shao, M. Deprotonated of layered double hydroxides during electrocatalytic water oxidation for multi-cations intercalation. *Smart Mol.* **2024**, *2* (2), No. e20230026.
(33) Zhang, W.; Ge, W.; Qi, Y.; Sheng, X.; Jiang, H.; Li, C. Surfactant Directionally Assembled at the Electrode-Electrolyte Interface for Facilitating Electrocatalytic Aldehyde Hydrogenation. *Angew. Chem.* **2024**, *136*, No. e202407121.
(34) Kong, K.; Li, A.-Z.; Wang, Y.; Shi, Q.; Li, J.; Ji, K.; Duan, H. Electrochemical carbon-carbon coupling with enhanced activity and racemate stereoselectivity by microenvironment regulation. *Nat. Commun.* **2023**, *14* (1), 6925.
(35) Liu, C.; Li, R.; Zhou, W.; Liang, Y.; Shi, Y.; Li, R.-L.; Ling, Y.; Yu, Y.; Li, J.; Zhang, B. Selectivity origin of organic electrosynthesis controlled by electrode materials: a case study on pinacols. *ACS Catal.* **2021**, *11* (14), 8958−8967.
(36) Liu, H.; Patel, D. M.; Chen, Y.; Lee, J.; Lee, T.-H.; Cady, S. D.; Cochran, E. W.; Roling, L. T.; Li, W. Unraveling electroreductive mechanisms of biomass-derived aldehydes via tailoring interfacial environments. *ACS Catal.* **2022**, *12* (22), 14072−14085.
(37) Gutiérrez-Sánchez, O.; Daems, N.; Bulut, M.; Pant, D.; Breugelmans, T. Effects of benzyl-functionalized cationic surfactants on the inhibition of the hydrogen evolution reaction in CO2 reduction systems. *ACS Appl. Mater. Interfaces* **2021**, *13* (47), 56205−56216.
(38) Banerjee, S.; Han, X.; Thoi, V. S. Modulating the electrode-electrolyte interface with cationic surfactants in carbon dioxide reduction. *ACS Catal.* **2019**, *9* (6), 5631−5637.
(39) Yuan, X.; Lee, K.; Bender, M. T.; Schmidt, J.; Choi, K. S. Mechanistic Differences between Electrochemical Hydrogenation and Hydrogenolysis of 5-Hydroxymethylfurfural and Their pH Dependence. *ChemSusChem* **2022**, *15* (17), No. e202200952.
(40) Khanipour, P.; Löffler, M.; Reichert, A. M.; Haase, F. T.; Mayrhofer, K. J.; Katsounaros, I. Electrochemical Real-Time Mass Spectrometry (EC-RTMS): Monitoring Electrochemical Reaction Products in Real Time. *Angew. Chem.* **2019**, *131* (22), 7351−7355.
(41) Asfia, M. P.; Cuomo, A.; Kloth, R.; Mayrhofer, K. J.; Nikolaienko, P. The Role of Alkali Cations on the Selectivity of 5-Hydroxymethylfurfural Electroreduction on Glassy Carbon. *ChemSusChem* **2024**, *17* (20), No. e202400535.
(42) Peirow Asfia, M.; Parada, W. A.; Klerner, L.; Cuomo, A.; Sajevic, U.; Mayrhofer, K. J.; Nikolaienko, P. Improved Mass Transport of 5-Hydroxymethylfurfural Electrochemical Reduction through Gas-Liquid Cocirculation. *ACS Sustainable Chem. Eng.* **2025**, *13*, 12323.
(43) Ge, W.; Chen, Y.; Fan, Y.; Zhu, Y.; Liu, H.; Song, L.; Liu, Z.; Lian, C.; Jiang, H.; Li, C. Dynamically Formed Surfactant Assembly at the Electrified Electrode-Electrolyte Interface Boosting CO(2) Electroreduction. *J. Am. Chem. Soc.* **2022**, *144* (14), 6613−6622.
(44) De, S.; Aswal, V. K.; Goyal, P. S.; Bhattacharya, S. Role of spacer chain length in dimeric micellar organization. Small angle neutron scattering and fluorescence studies. *J. Phys. Chem.* **1996**, *100* (28), 11664−11671.
(45) Zhang, X.; Yan, X.; Chen, P.; Zhang, P.; Kang, X.; Ma, J.; Chen, C.; Han, B. Selective and Efficient CO(2) Electroreduction to Formate on Copper Electrodes Modified by Cationic Gemini Surfactants. *Angew. Chem., Int. Ed. Engl.* **2024**, *63* (9), No. e202315822.

https://doi.org/10.1021/acssuschemeng.5c04330
ACS Sustainable Chem. Eng. 2025, 13, 17151−17160